Applied Catalysis B: Environmental 126 (2012) 334–341

Contents lists available at SciVerse ScienceDirect

Applied Catalysis B: Environmental

journal homepage: www.elsevier.com/locate/apcatb

Photocatalytic properties of TiO_2/WO_3 coatings formed by plasma electrolytic oxidation of titanium in 12-tungstosilicic acid

S. Stojadinović[a,*], N. Radić[b], R. Vasilić[c], M. Petković[a], P. Stefanov[d], Lj. Zeković[a], B. Grbić[b]

[a] University of Belgrade, Faculty of Physics, Studentski trg 12-16, 11000 Belgrade, Serbia
[b] University of Belgrade, Institute of Chemistry, Technology and Metallurgy, Department of Catalysis and Chemical Engineering, Njegoševa 12, 11000 Belgrade, Serbia
[c] Faculty of Environmental Governance and Corporate Responsibility, Educons University, Vojvode Putnika 87, Sremska Kamenica, Serbia
[d] Institute of Physical Chemistry, Bulgarian Academy of Sciences, Sofia 1113, Bulgaria

ARTICLE INFO

Article history:
Received 16 June 2012
Received in revised form 21 July 2012
Accepted 31 July 2012
Available online 7 August 2012

Keywords:
Photocatalysis
Plasma electrolytic oxidation
TiO_2/WO_3
TiO_2

ABSTRACT

In this paper, we have investigated photocatalytic properties of TiO_2/WO_3 coatings formed by plasma electrolytic oxidation (PEO) of titanium in 12-tungstosilicic acid water solution and compared with photocatalytic activity of pure TiO_2 coatings. The photocatalytic activity of the coatings is evaluated by measuring the degradation of methyl orange under simulated sunlight conditions. Photocatalytic activity of TiO_2/WO_3 coatings varied with duration of PEO process and higher photoactivity is obtained for a shorter process time. Photocatalytic activity of TiO_2/WO_3 coatings is related to morphology and phase and elemental composition of coatings. The oxide coatings morphology is strongly dependent on PEO time. The elemental components of the coatings are Ti, W and O. The oxide coatings are partly crystallized and mainly composed of WO_3 and anatase. Decrease in the number of microdischarge channels and agglomeration of particles on the surface leads to a decrease in photocatalytic activity. The reduction of the photocatalytic activity with increased time of PEO process is accompanied with the increase of WO_3 concentration on the coatings' surface. Diffuse reflectance spectroscopy has shown that coatings enriched with tungsten oxide exhibit significant red shift with respect to the pure TiO_2 coatings. TiO_2/WO_3 coatings with improved catalytic activity, compared to pure TiO_2 coatings, are grouped around energy band gap of 2.6 eV. The results of PL measurements of TiO_2/WO_3 coatings are in agreement with photocatalytic activities. The increase of PL intensity corresponds to decrease of photocatalytic activity of the coatings, indicating fast recombination of electron–hole pairs.

1. Introduction

Plasma electrolytic oxidation (PEO), also called microarc oxidation (MAO) or anodic spark deposition (ASD), is high-voltage anodizing process which produces a stable oxide coating on the surfaces of number of metals, such as aluminum, magnesium, titanium, zirconium, tantalum, and their alloys [1–4]. Oxide coatings have controllable morphology and composition, excellent bonding strength to the metal, high microhardness, high-quality wear and corrosion resistance, etc. PEO process involves anodization of metals above the dielectric breakdown voltage where numerous transient, fine, short-lived discharges are generated continuously over the coating surface, accompanied by gas evolution [5,6]. Plasma-chemical, thermal, and anodic oxidation processes are induced at the discharge sites due to increased local temperature and pressure modifying the structure, composition, and morphology of such oxide coatings. The oxide coatings formed by PEO usually contain crystalline and amorphous phases with constituent species originating both from metal and electrolyte.

Titanium dioxide (TiO_2) coatings obtained by PEO process of titanium have been widely investigated because of their potential applications, including biocompatible materials, structural ceramics, photocatalysis, sensors, optical coatings, etc. [7–11]. TiO_2 is an excellent photocatalyst, which causes the degradation of various organic pollutants under UV light irradiation due to its relatively wide band gap (~3.2 eV) [12]. This wide band gap suggests that TiO_2 can only be excited by high energy UV irradiation with a wavelength below 387 nm. This practically rules out the use of sunlight as an energy source for the photoreaction. Also, a high rate of recombination between excited electron/hole pairs limits the photocatalytic activity. Recently, a lot of research has been focused on improving the TiO_2 photocatalytic activity, increasing the absorption of TiO_2 under visible irradiation and decreasing electron/hole recombination rate. It has been reported that the efficiency of a photocatalytic reaction can be improved by coupling TiO_2 with other semiconducting materials, such as CdSe [13], CdS [14], SnO_2 [15], WO_3 [16], ZrO_2 [17], and V_2O_5 [18].

* Corresponding author. Tel.: +381 11 7158161; fax: +381 11 3282619.
E-mail address: sstevan@ff.bg.ac.rs (S. Stojadinović).

0926-3373/$ – see front matter © 2012 Elsevier B.V. All rights reserved.
http://dx.doi.org/10.1016/j.apcatb.2012.07.031

Up to now, several papers focused on the investigation of photocatalytic activity of TiO_2/WO_3 composites prepared by different processes such as hydrothermal [19], sol–gel [20], impregnation methods [21], and microarc oxidation [22]. This research is triggered by the fact that the band gap of WO_3 is 2.4–2.8 eV and both the upper edge of the valence band and the lower edge of the conduction band of WO_3 are lower than those of TiO_2. Thus, WO_3 can be excited by illumination with visible light. Bi-component WO_3 and TiO_2 materials have shown enhanced photocatalytic activity with respect to their plain component analogs, since their valence and conduction band energy diagrams [23] favor electron injection from the conduction band of TiO_2 to that of WO_3 and hole transfer between valence bands in the opposite direction. This, in turn, reduces electron–hole recombination in both semiconductors [23].

In the present work we used economic, efficient, and environmentally benign PEO process to form TiO_2/WO_3 coatings on titanium substrate. As electrolyte we used 12-tungstosilicic acid (WSiA). WSiA is one of the best known heteropoly acids with Keggin anion structure and with low temperature structural phase transition (535 °C) [24]. In some cases, iso- and heteropolyoxotungstic acids have been used for formation of tungsten oxide by PEO process on titanium and other valve metals [25,26]. During the PEO process, under high temperature inside discharge channels, thermal decomposition of WSiA results in tungsten oxide structures on the substrate [3,4,27].

The main advantage of using the PEO method in producing TiO_2/WO_3 binary semiconductor oxide catalysts is a very short time of anodization caused by skipping the annealing step, which is required in to transform amorphous TiO_2 into crystalline phase (for example see references in reviews of Lianos [28] and Georgieva [29]). During the PEO, high temperature regions (from ~2000 K to ~10,000 K) are formed all over the samples' surface, transforming amorphous TiO_2 into its crystalline phase, making the post-deposition annealing unnecessary. Furthermore, if PEO method is compared to other electrochemical methods [30–32], no two-bath setups, deaeration, and/or potential control during the photocatalysis is required. These peculiarities are rendering the PEO method for producing TiO_2/WO_3 catalysts highly desirable for industrial application due to its efficiency.

Atomic force microscopy (AFM), scanning electron microscopy (SEM), diffuse reflectance spectroscopy (DRS), photoluminescence (PL), X-ray diffraction (XRD), and X-ray photoelectron spectroscopy (XPS) were used as tools to characterize obtained oxide coatings. Methyl orange (MO) is selected as a model compound in order to estimate the photocatalytic activity of oxide coatings formed by PEO of titanium in WSiA.

2. Experimental details

Rectangular samples of dimensions 25 mm × 10 mm × 0.25 mm of 99.5% purity titanium were used as working electrodes in the experiment. The working electrodes were sealed with insulation resin leaving only active surface with an area of 1.5 cm^2. Before the anodization, samples were degreased in acetone, ethanol, and distilled water, using ultrasonic cleaner, and dried in a warm air stream. The anodization process was carried out in an electrolytic cell [33]. Two platinum wires (5 cm long and 1 mm in diameter) were used as cathodes. The power supply was a homemade DC power unit providing voltages of 0–600 V and a current of 0–500 mA. During the anodization, the electrolyte circulated through the chamber–reservoir system, and the control temperature sensor was situated immediately by the sample. The temperature of the electrolyte was maintained during the anodization process at (20 ± 1) °C. We have anodized titanium in water solution 10^{-3} M WSiA ($H_4SiW_{12}O_{40}$). The electrolyte was prepared by using double distilled and deionized water and PA (pro analysis) grade chemical compound. In addition, some samples were anodized in water solution of 10 g/L Na_3PO_4 to obtain pure TiO_2 layer by PEO process. Anodizing was carried out at current density of 150 mA/cm^2. After the anodization, samples were rinsed in distilled water to prevent additional deposition of electrolyte components during drying.

The topography and roughness of oxide coatings were characterized using an atomic force microscope (AFM; Veeco Instruments, model Dimension V). Micrographs were obtained in tapping mode under ambient conditions, using TAP300 tips (resonant frequency 300 kHz, force constant 40 N/m). Roughness data were obtained using diNanoScope software (version 7.0).

Scanning electron microscope (SEM) JEOL 840A equipped with energy dispersive X-ray spectroscopy (EDX) was used to characterize morphology and chemical composition of formed oxide coatings.

The crystallinity of samples was analyzed by XRD, using a Phillips PW 1050 powder diffractometer in Bragg–Brentano geometry, with Ni-filtered Cu K_α radiation (λ = 1.54178 Å). Diffraction data were acquired over scattering angle 2θ from 15° to 75° with a step of 0.050° and acquisition time of 1 s/step.

The surface composition of the oxide coatings was determined by X-ray photoelectron spectroscopy (XPS) using a VG ESCALAB II electron spectrometer under a base pressure of 1×10^{-8} Pa. The photoelectron spectra were excited using nonmonochromatized Al K_α radiation ($h\nu$ = 1486.6 eV) with a total instrumental resolution of 1 eV. The C 1s line of the adventitious carbon at 285 eV was used as an internal standard to calibrate the binding energies. The photoelectron spectra were corrected by subtracting a Shirley-type background and were quantified using the peak area and Scofield photoionization cross-sections.

UV–Vis diffuse reflectance spectra (DRS) of oxide coatings were recorded using UV–Vis spectrophotometer (Specord M40 Carl Zeiss). Photoluminescence (PL) spectral measurements were taken on a Horiba Jobin Yvon Fluorolog FL3-22 spectrofluorometer, with Xe lamp as the excitation light source at room temperature. The obtained spectra were corrected for the spectral response of the measuring system and spectral distribution of the Xe lamp.

Photocatalytical activity of TiO_2/WO_3 coatings was determined by degrading MO at room temperature. Samples of dimensions 15 mm × 10 mm (active surface) were immersed into 10 mL of 8 mg/L aqueous MO solution. Catalyst foil in the photocatalytic reactor was placed on perforated holder, 5 mm above the bottom of the reactor, with magnetic stirrer under the holder. Prior to illumination, the solutions and the catalyst were magnetically stirred in the dark for 30 min to achieve adsorption–desorption equilibrium. The MO solution was then irradiated under lamp that simulates solar radiation (Solimed BH Quarzlampen), with a power consumption of 300 W, housed 25 cm above the top surface of the solution. Illumination intensity on the top of the photocatalytic reactor was 850 lx. A fixed quantity of the MO solution was removed every 2 h to measure the absorption and then concentration, using UV-VIS spectrometer (Thermo Electron Nicolet Evolution 500). After each measurement of MO concentration probe solution was returned back to the photocatalytic reactor. MO has a maximum absorbance at 464 nm, which was used as a wavelength for monitoring MO degradation. The absorbance was converted to the MO concentration in accordance with a standard curve showing a linear relationship between the concentration and the absorbance at this wavelength. Prior to the photocatalysis, the MO solution was tested for photolysis in the absence of the photocatalyst in order to examine its stability. The lack of change in the MO concentration after 8 h of irradiation revealed that the MO was stable under applied conditions and that degradation was only due to the presence of

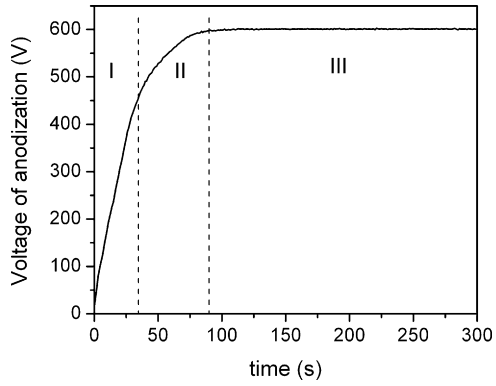

Fig. 1. Time variation of voltage during galvanostatic anodization of titanium in 10^{-3} M WSiA at 150 mA/cm^2.

the photocatalyst. The reproducibility of the results was verified by performing each test several times.

3. Results and discussion

3.1. Anodization of titanium

Typical voltage–time curve during anodization of titanium in 10^{-3} M WSiA at constant current density of 150 mA/cm^2 is shown in Fig. 1. Based on the voltage–time response, the PEO process can be divided in three stages. From the beginning of anodization, the voltage increases approximately linearly with time to about 460 V, resulting in the constant rate of increase of the barrier oxide film thickness (stage I). In this stage main part of the total current passing through the barrier oxide film is ionic current ensuring the increase of the oxide film's thickness. During anodization electrons are injected into the conduction band of the anodic oxide and accelerated by the electric field producing avalanches by an impact ionization mechanism [34]. When the avalanche of electronic current reaches critical value the breakdown occurs [35]. This stage is followed by apparent deflection from linearity in voltage–time curve (stage II). After the breakdown, voltage continually increases, but the voltage–time slope decreases and a large number of small size microdischarges appear, evenly distributed over the whole sample surface (Fig. 2). Further anodization results in relatively stable value of the voltage of anodization (stage III). The size of microdischarges becomes larger, while spatial density of microdischarges becomes lower, with increasing time of PEO process.

3.2. Surface morphology, chemical and phase composition of TiO_2/WO_3 coatings

PEO is a complex process combining concurrent partial processes of oxide formation, dissolution and dielectric breakdown [36]. At the beginning of the titanium anodization, oxide layer grows at the titanium/oxide and oxide/electrolyte interfaces as a result of migration of O^{2-}/OH^- and Ti^{4+} ions across the oxide assisted by a strong electric field. Initial oxide layer forms at the surface of titanium as a result of the following overall reaction:

$$Ti + 2H_2O - 4e^- \rightarrow TiO_2 + 4H^+ + 4e^-. \quad (1)$$

During the whole PEO process anionic components of the electrolyte, Keggin anions $[SiW_{12}O_{40}]^{4-}$, are drawn toward the anode. As breakdown through microdischarges starts, high temperatures and pressures are developed locally on the surface, resulting in decomposition of 12-tungstosilicic acid according to:

$$H_4SiW_{12}O_{40} \rightarrow H_2SiO_3 + 12WO_3 + H_2O \quad (2)$$

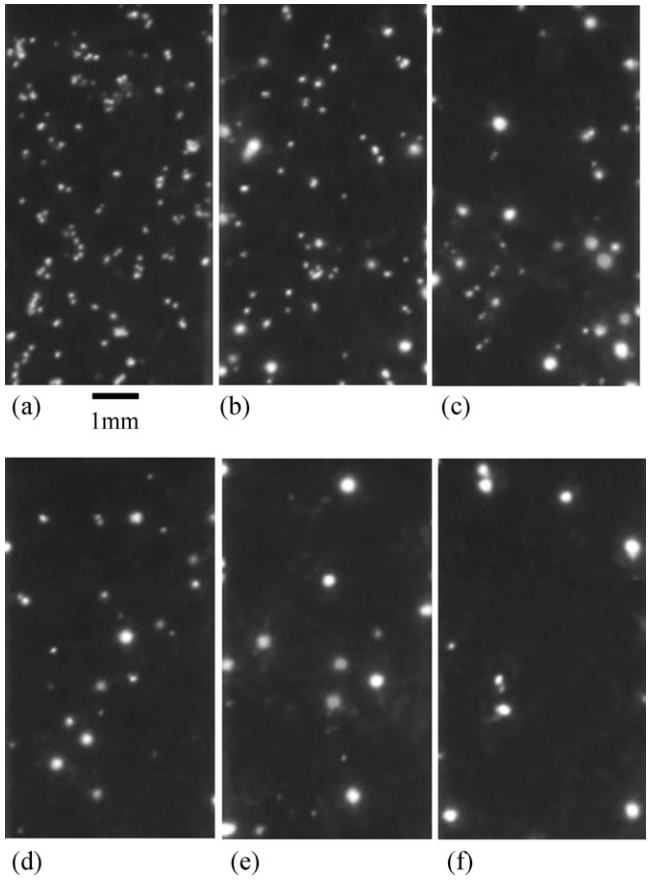

Fig. 2. Microdischarges appearance at various stages of PEO process in WSiA: (a) 30 s; (b) 60 s; (c) 90 s; (d) 180 s; (e) 300 s; (f) 600 s.

Under these conditions, solid WO_3 deposits along with TiO_2 on the growing oxide surface. It should be noted that mixed TiO_2/WO_3 layer is grown on pure TiO_2 layer, previously formed only by anodic oxidation. Therefore, TiO_2/WO_3 coatings are composed of two components which come from different sources. TiO_2 originates from substrate, while WO_3 deposits from the electrolyte. Having this in mind, it can be expected that at different stages of PEO process surface composition of coatings changes. At the beginning of the PEO process, pure TiO_2 layer forms but as PEO process proceeding the coating is gradually enriched with WO_3. Ti dissolution from Ti substrate and transfer on the surface is hindered by increased coating thickness, while outer surface is readily accessible for Keggin anions decompositions and WO_3 deposition. It is also worth mentioning that colloidal silicic acid, formed by decomposition of Keggin anion, is mainly negatively charged in the mild acidic as well as in alkaline environment. However, in the strong acidic medium which exists in oxide/electrolyte interfaces (Eq. (1)), colloidal silicic acid becomes positively charged and may be ejected from the microdischarge channels into the electrolyte by electrostatic forces [37].

Results of EDS analysis of TiO_2/WO_3 surface coatings formed in various stages of PEO process in WSiA (Fig. 3) are shown in Table 1. Coatings are consisted only of Ti, W and O. Absence of silicon is in agreement with proposed mechanism of PEO process. Also, amount of tungsten in oxide coatings increases with PEO time while the amount of titanium decreases.

SEM micrographs of TiO_2/WO_3 coatings formed in various stages of PEO process in WSiA are shown in Fig. 3. After the breakdown oxide surface becomes lacy with a number of microdischarge channels as well as molten regions formed due to rapid cooling effect of

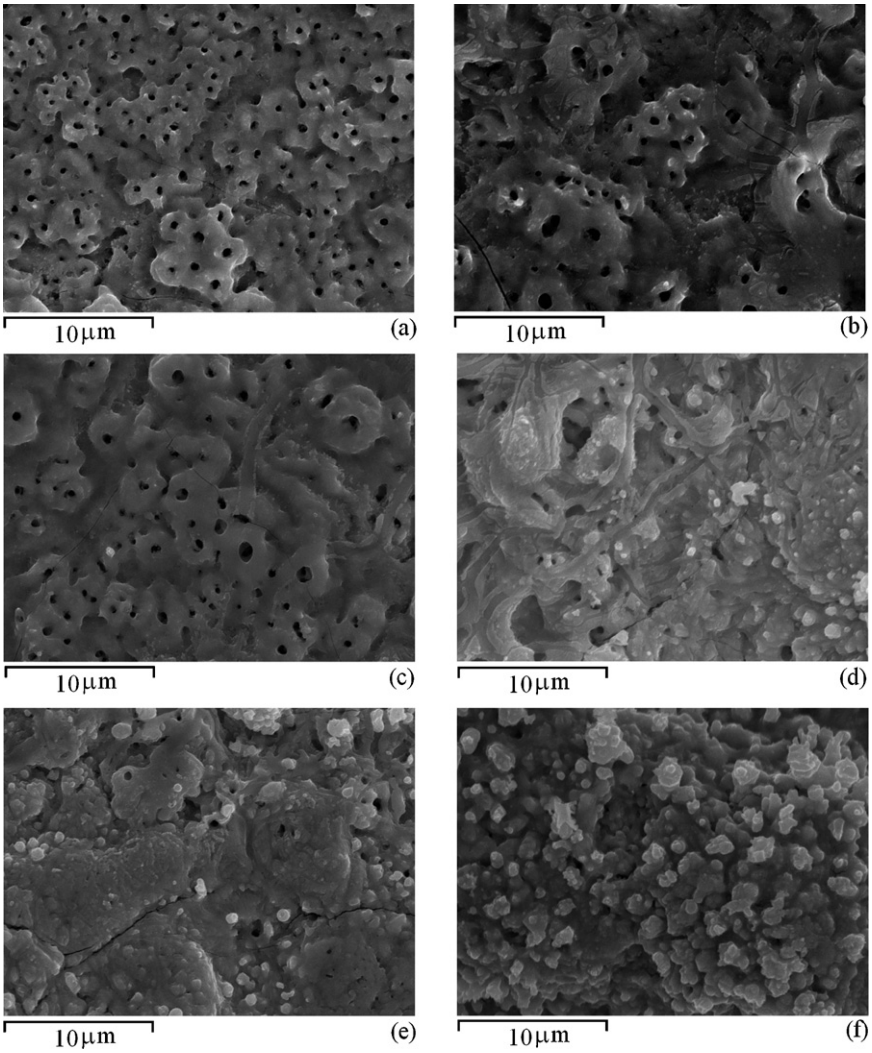

Fig. 3. SEM micrographs of TiO_2/WO_3 coatings formed in various stages of PEO process in WSiA: (a) 30 s; (b) 60 s; (c) 90 s; (d) 180 s; (e) 300 s; (f) 600 s.

the electrolyte. Microdischarges are generated by dielectric breakdown through weak sites in the oxide coating. The number of weak sites is reduced with increasing time of PEO process, i.e. with increasing thickness of the oxide coating. The increased size of microdischarges with increasing time of PEO (Fig. 2) is ascribed to reduced number of discharging sites through which higher anodic current is able to pass [38]. The surface morphology evolution of the coatings formed on titanium during the PEO process clearly demonstrates the decrease in the number of micropores and their increase in size (Fig. 3). In a thicker layer of oxide coating, higher energy is required for the current to pass through the coating. Under this condition, the current is localized at weak points of the layer formed to find its way through the coating. This is the reason why the diameter of the discharge channel increases. Also, thicker coatings have higher surface roughness. Fig. 4 shows the surface topography of oxide coatings in various stages of PEO process. In initial stage of PEO process (Fig. 4a), discharge channels are well distributed and TiO_2/WO_3 coatings exhibit lower surface roughness (~140 nm). As the number of discharge channels decreases with time of PEO, non-uniformities in the oxide coatings appear causing an increase in surface roughness (~520 nm for sample in Fig. 4e).

Table 1
EDS analysis of TiO_2/WO_3 surface coatings in Fig. 3.

Sample	PEO time [s]	Atomic [%]			W:Ti
		O	Ti	W	
Fig. 3a	30	77.94	10.18	11.88	1.1
Fig. 3b	60	78.60	8.31	13.09	1.6
Fig. 3c	90	78.85	6.98	14.17	2.0
Fig. 3d	180	77.66	6.22	16.12	2.6
Fig. 3e	300	78.75	4.09	17.16	4.2
Fig. 3f	600	80.60	1.27	18.13	14.3

The XRD patterns of TiO_2/WO_3 coatings formed in various stages of PEO process in WSiA are shown in Fig. 5. For the sake of comparison pure TiO_2 coating formed during PEO process of titanium in Na_3PO_4 is presented in Fig. 5g. The coatings are partly crystallized and mainly composed of WO_3 and TiO_2 (anatase). It is evident that increasing time of PEO process results in enrichments of coatings with WO_3. Elemental Ti mainly originates from the substrate and its intensity decreases with prolonged time of PEO process indicating increase of coatings thickness. These results are in accordance with EDS data (Table 1) and support proposed mechanism of coating growth.

3.3. Photocatalytic activity of TiO_2/WO_3 coatings

Photocatalytic activity in MO photodegradation for TiO_2/WO_3 coatings along with pure TiO_2 coating is presented in Fig. 6. Photocatalytic activity of TiO_2/WO_3 coatings varies with the duration

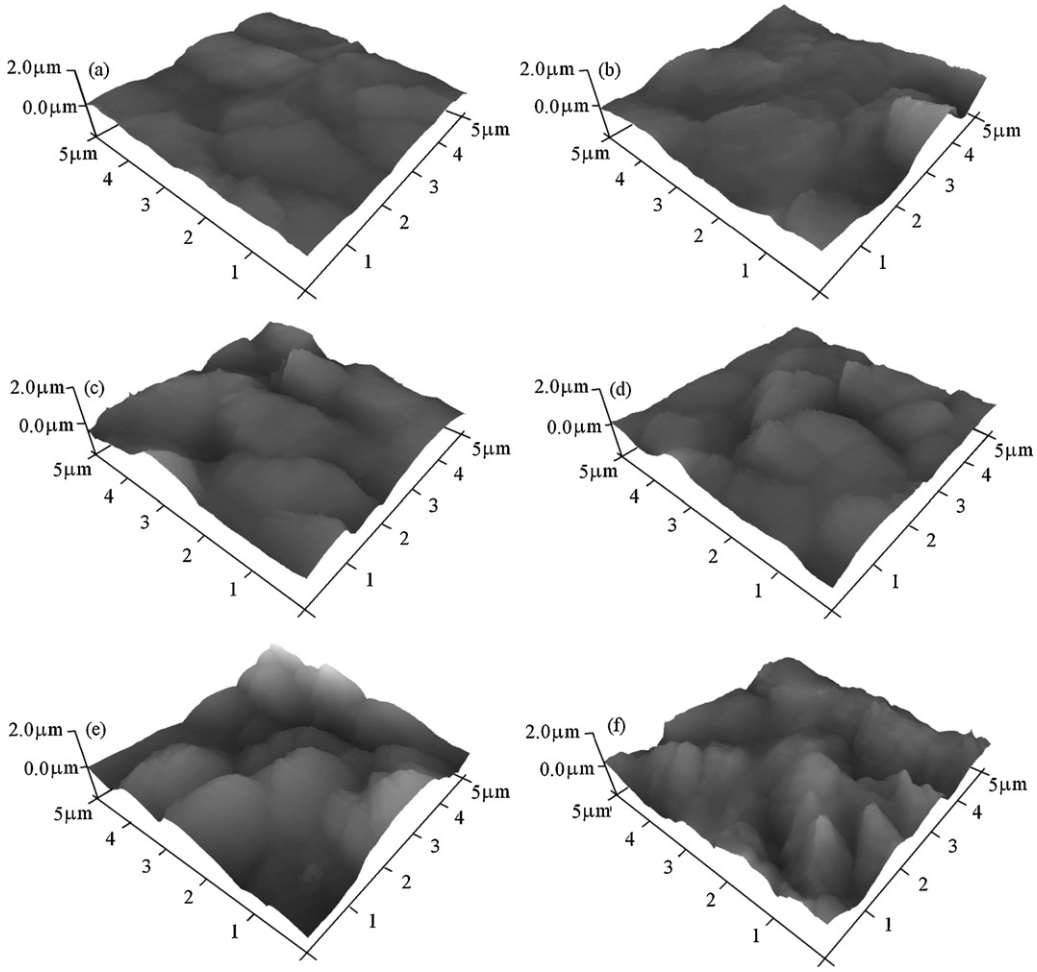

Fig. 4. Three-dimensional AFM images of TiO_2/WO_3 coatings formed in various stages of PEO process in WSiA: (a) 30 s; (b) 60 s; (c) 90 s; (d) 180 s; (e) 300 s; (f) 600 s.

of PEO process; an increase in the PEO time results in decreased photocatalytic activity. Fig. 6 clearly indicates that some TiO_2/WO_3 coatings exceed the photocatalytic activity of pure TiO_2 coating. These improved activities are related to shorter times of PEO process (30 s, 60 s and 90 s). On the other hand, increased duration of PEO process (180 s, 300 s and 600 s) significantly deteriorates photocatalytic activity, yielding activities lower than those of pure TiO_2 catalyst. Based on our experimental findings, activities can be related to morphology of TiO_2/WO_3 coatings (SEM and AFM) and phase and elemental composition (XRD and EDS). It is evident that decrease in the number of microdischarge channels (Fig. 2) and/or agglomeration of particles on the surface (Fig. 3) leads to a decrease in activity. Also, the reduction in the photocatalytic activity with increasing time of PEO process can be attributed to the rise of WO_3 concentration in the coatings. TiO_2/WO_3 coatings with improved photocatalytic activity with respect to pure TiO_2 are synthesized within the stage II of the PEO process, where the density of microchannels (Fig. 3a–c) follows the density of sparks (Fig. 2a–c). TiO_2/WO_3 coatings with lower activity originate from the stage III of PEO process, where voltage of anodization is constant. Stage III is

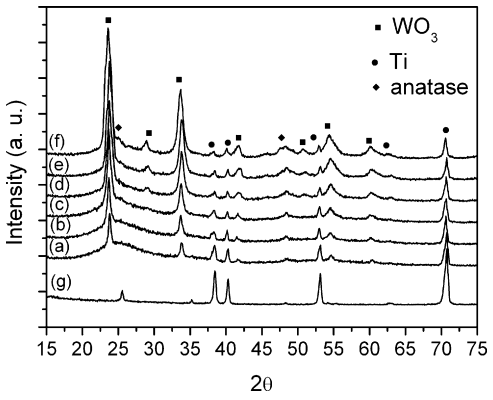

Fig. 5. XRD patterns of TiO_2/WO_3 coatings formed in various stages of PEO process in WSiA: (a) 30 s; (b) 60 s; (c) 90 s; (d) 180 s; (e) 300 s; (f) 600 s; (g) TiO_2.

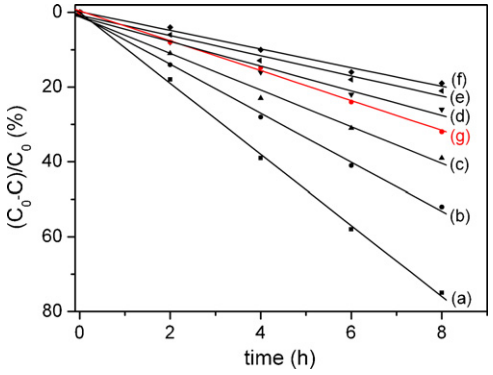

Fig. 6. Photocatalytic performance of TiO_2/WO_3 coatings formed in various stages of PEO process in WSiA: (a) 30 s; (b) 60 s; (c) 90 s; (d) 180 s; (e) 300 s; (f) 600 s; (g) TiO_2.

Table 2
XPS data of elemental surface concentrations.

PEO time	Atomic [%]			W:Ti
	O	Ti	W	
30 s in Na_3PO_4	80.2	19.8	0.0	0
30 s in WSiA	73.0	10.1	16.9	1.7
60 s in WSiA	73.7	9.5	16.8	1.8
90 s in WSiA	75.3	8.4	16.3	1.9
180 s in WSiA	73.0	8.2	18.8	2.3
300 s in WSiA	74.3	6.3	19.4	3.1

characterized by lower density of sparks (Fig. 2d–f) and disappearance of well distinguished microchannels due to surface coverage by large particle agglomerates.

Results of elemental analysis of surface coatings (EDS, Table 1) indicate strong influence of W:Ti ratio on photocatalytic activity. The highest activity is associated to W:Ti ratio close to 1. Increased time of PEO process increases W:Ti ratio and decreases the activity of TiO_2/WO_3 coatings. Ratio of W:Ti close to 1 leads us to assumption that the rate of Ti dissolution from the substrate is close to the rate of decomposition of Keggin anion i.e. rate of WO_3 deposition, leading to the formation of TiO_2/WO_3 solid solution on the surface. In this manner it could be considered that solid solution TiO_2/WO_3 is formed on the surface. XPS measurements could offer deeper inside into such assumption. The XPS surface composition of the coatings, Table 2, was determined using the W 4d peaks instead of W 4f peaks due to overlapping between the W 4f peaks and the Ti 3p peak. The ratio W:Ti shows the same trend as ratio obtained by EDS analysis, i.e., it increases with time of PEO process.

Fig. 7 shows the XPS spectra recorded for the oxide coatings formed in various stages of PEO process. The measured binding energy of the W $4f_{7/2}$ peak for all samples is at about 36.2 eV (Fig. 7i) and it corresponds to tungsten in the W^{6+} oxidation state (WO_3) [39]. The binding energy of W $4d_{5/2}$ peak at 248.0 eV (Fig. 7ii) is also characteristic for W^{6+} oxidation state [40]. The Ti 2p photoelectron spectrum obtained for the pure TiO_2 coating shows the spin–orbit components ($2p_{3/2}$ and $2p_{1/2}$) at 458.9 eV and 464.8 eV, respectively, assigned to Ti^{4+} ions in TiO_2 (Fig. 7iii,f). For all TiO_2/WO_3 coatings a little positive shift of the binding energy of Ti 2p lines by 0.3 eV is observed (Fig. 7iii,a–e). This shift could be explained with an interaction between the TiO_2 and WO_3 phases.

The valence band (VB) spectra of the TiO_2/WO_3 coatings have been also analyzed, finding a clear evidence for the band gap narrowing. Fig. 8 compares the valence band spectra of TiO_2 and TiO_2/WO_3 formed by PEO process for 180 s. The valence band of pure TiO_2 has mainly O 2p character and its upper edge is located at approximately 3.0 eV. The valence band of WO_3 is characterized with a maximum located at about 7 eV, corresponding to a "W 5d–O 2p" band hybridized states [41]. The valence band spectrum of TiO_2/WO_3 in Fig. 8 exhibits predominately WO_3 structure with an upper edge located at ~2.5 eV.

The XPS elemental analysis is more representative measure of surface composition than EDS analysis, because XPS represents thickness of about 10 nm compared to few hundred nm measured by EDS. Consequently, that might be a reason for differences between EDS and XPS ratios of W:Ti. Another question arises from this consideration, which analysis is more adequate for interpretation of photocatalytic activity. Regardless of the morphology, surface area and pore size, light most likely exceeds depth of 10 nm and penetrates to the deeper coating layers. Therefore, light as immaterial reagent in MO photodegradation reacts, on its path from the top to the bottom of the coatings, with different active centers. Nature of these centers is changing along the light path; from pure TiO_2 on the bottom of the coating, via solid solution of TiO_2/WO_3, and with dominant WO_3 layer on the top. Contribution

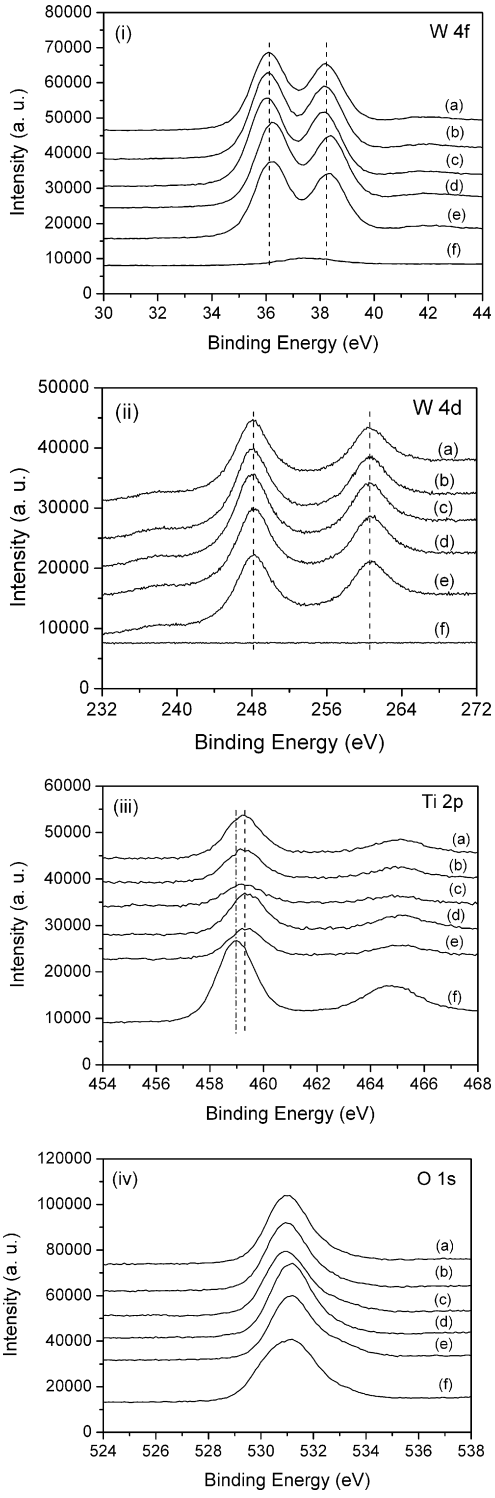

Fig. 7. High resolution XPS spectra of TiO_2/WO_3 coatings: (i) W 4f; (ii) W 4d; (iii) Ti 2p; (iv) O 1s; formed in various stages of PEO process in WSiA: (a) 30 s; (b) 60 s; (c) 90 s; (d) 180 s; (e) 300 s; (f) TiO_2.

of particular centers to overall activity is influenced by the thickness of the coatings i.e. by time of PEO process. Thus, variations between inner (bottom) and outer (top) part of coatings are more pronounced for thicker coatings, decreasing "effectiveness factor". The ambiguities on correlation between photocatalytic activity and XPS and EDS data could be suppressed by investigation of optical properties of TiO_2/WO_3 coatings. Same as for photocatalytic activity, diffuse reflectance spectroscopy (DRS) and photoluminescence

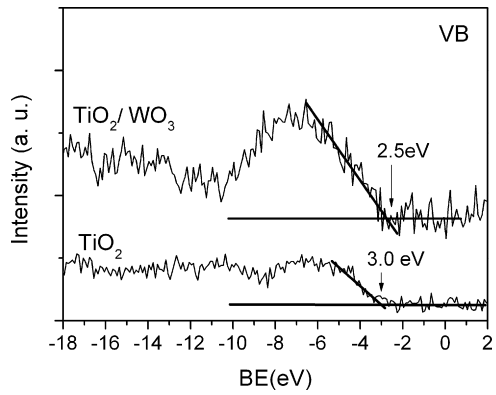

Fig. 8. XPS valence band spectra of TiO_2 and TiO_2/WO_3 formed by PEO process for 180 s.

spectroscopy can shed more light on the complex interaction of light with layers consisting of various active centers and differently structured coatings.

Fig. 9 shows DRS spectra of TiO_2/WO_3 coatings formed in various stages of PEO process. Also, pure titanium oxide coating obtained by the same process is presented in Fig. 9. The spectra show a band edge in the region from 370 nm to 420 nm that is attributed to photo excitation from valence band to conduction band. The samples with tungsten oxide exhibit significant red shift with respect to the pure TiO_2. Shift to the higher wavelengths follows duration of PEO process. Consequently, band gap *Eg* (eV) gradually decreases from 3.0 eV for pure TiO_2 to 2.5 eV for TiO_2/WO_3 formed by PEO process for 600 s. Band gap, *Eg* (eV), is calculated according to simple equation:

$$Eg\ (\mathrm{eV}) = \frac{1240}{\lambda} \tag{3}$$

where λ (nm) is wavelength. Samples of TiO_2/WO_3 with improved catalytic activity compared to pure TiO_2 (Fig. 6) are grouped around energy band gap of 2.6 eV.

Red-shifts of absorption wavelength range of TiO_2/WO_3 could be attributed to the formation of new energy levels due to formation of W–O–Ti bonds in the solid solution of TiO_2/WO_3 during PEO process [42]. DRS spectra for TiO_2/WO_3 coatings formed by PEO process for 180 s, 300 s, and 600 s are further moved to red side with respect to TiO_2. Although useful spectral region for photocatalysis is expanded, poor photocatalytic activity is observed. Energy band gap of about 2.55 eV is in accordance with XPS results (Fig. 8) of valence band spectra of TiO_2/WO_3 formed by PEO process for 180 s, indicating predominant contribution of WO_3 to photocatalytic reaction. Probably, prolonged PEO process forms thicker

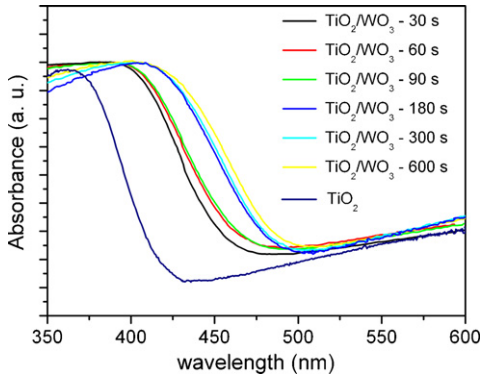

Fig. 9. Diffuse reflectance spectra of TiO_2/WO_3 coatings formed in various stages of PEO process.

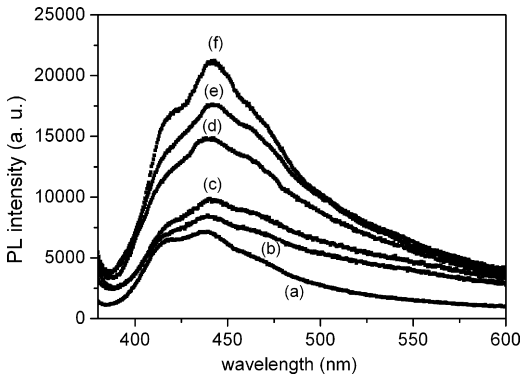

Fig. 10. PL spectra of TiO_2/WO_3 coatings formed in various stages of PEO process in WSiA: (a) 30 s; (b) 60 s; (c) 90 s; (d) 180 s; (e) 300 s; (f) 600 s.

TiO_2/WO_3 coatings with low effectiveness factor, making deeper layers of coatings inaccessible to light.

Confirmation of such assumption is given by photoluminescence (PL) spectra. PL emission spectra of TiO_2/WO_3 coatings formed in various stages of PEO process are shown in Fig. 10. The PL spectral measurements have been widely used to investigate the structure and properties of the active sites on the surface of metal oxides because of its high sensitivity and nondestructive character. Also, the PL technique has been useful in the field of photocatalysis. Information such as surface oxygen vacancies and defects, as well as the efficiency of charge carrier trapping, immigration and transfer can be obtained [43]. The increase of PL intensity corresponds to decrease of photocatalytic activity of the coatings, indicating fast recombination of electron–hole pairs. PL results are in agreement with photocatalytic activities (Fig. 6). Coatings formed in stage II of PEO process (30 s, 60 s and 90 s) show lower PL intensity and follows order of photoactivities. Improvement in photoactivity is achieved by significant contribution of TiO_2/WO_3 centers which enables transfer of photo-generated electrons from TiO_2 to the lower lying conduction band of WO_3. The positive holes move toward the valence band of TiO_2, resulting in reduction of the electron–hole recombination rate [44]. High intensity of PL corresponds to coatings formed in stage III of PEO process (180 s, 300 s and 600 s) and photocatalytic activity lower than pure TiO_2. This result, along with DRS data, confirms significant participations of WO_3 centers in the reaction because conductance and valance bands of WO_3 are near each other resulting in a high electron–hole recombination rate.

4. Conclusions

Based on our experimental results it can be concluded that:

(1) Plasma electrolytic oxidation (PEO) of titanium in 12-tungstosilicic acid is economic and efficient process for forming TiO_2/WO_3 coatings with enhanced photocatalytic activity compared to pure TiO_2.
(2) Photocatalytic activity of TiO_2/WO_3 coatings varies with duration of PEO process. The increase of PEO time results in decreased photocatalytic activity. TiO_2/WO_3 coatings formed for shorter PEO times (up to 90 s) exceed activity of pure TiO_2 coatings, while increased duration of PEO process (above 150 s) significantly deteriorates the activity of TiO_2/WO_3 coatings and they became less active than pure TiO_2.
(3) Photocatalytic activity of TiO_2/WO_3 coatings is related to morphology and phase and elemental composition of coatings. The oxide coatings morphology is strongly dependent on PEO time. During the PEO of titanium density of discharge channels decreases while their diameter increases, resulting in

increased roughness of the oxide coatings. The elemental components of the coatings are Ti, W and O. Surface concentration of pinpointed elements changes during the PEO process. Concentration of W increases while Ti decreases with PEO time. The oxide coatings are partly crystallized and mainly composed of WO_3 and anatase. Decrease in the number of microdischarge channels and agglomeration of particles on the surface leads to a decrease in photocatalytic activity. Also, the reduction in the photocatalytic activity with increasing time of PEO process is accompanied with rise of WO_3 concentration in the coating.

(4) DRS spectra of TiO_2/WO_3 coatings formed in various stages of PEO process show a band edge in the region from 370 nm for pure TiO_2 to 420 nm for TiO_2/WO_3. The coatings with tungsten oxide exhibit significant red shift with respect to the pure TiO_2. Shift to the higher wavelengths follows duration of PEO process and consequently, band gap gradually decreases from 3.0 eV for pure TiO_2 to 2.5 eV for TiO_2/WO_3 formed by PEO process for 600 s. TiO_2/WO_3 coatings with improved catalytic activity are grouped around energy band gap of 2.6 eV.

(5) The results of PL measurement of TiO_2/WO_3 coatings are in agreement with photocatalytic activities. The increase of PL intensity corresponds to decrease of photocatalytic activity of the coatings, indicating fast recombination of electron–hole pairs.

Acknowledgments

The authors gratefully acknowledge A. Žekić for the help with SEM analysis. This work is supported by the Ministry of Education and Science of the Republic of Serbia under projects nos. 171035, 172022, and 172026.

References

[1] A.L. Yerokhin, X. Nie, A. Leyland, A. Matthews, S.J. Dowey, Surface & Coatings Technology 122 (1999) 73.
[2] R. Arrabal, E. Matykina, T. Hashimoto, P. Skeldon, G.E. Thompson, Surface & Coatings Technology 203 (2009) 2207.
[3] S. Stojadinović, R. Vasilić, M. Petković, Lj. Zeković, Surface & Coatings Technology 206 (2011) 575.
[4] M. Petković, S. Stojadinović, R. Vasilić, Lj. Zeković, Applied Surface Science 257 (2011) 10590.
[5] S. Stojadinović, R. Vasilić, M. Petković, I. Belča, B. Kasalica, M. Perić, Lj. Zeković, Electrochimica Acta 59 (2012) 354.
[6] L.O. Snizhko, A.L. Yerokhin, A. Pilkington, N.L. Gurevina, D.O. Misnyankin, A. Leyland, A. Matthews, Electrochimica Acta 349 (2004) 2085.
[7] Z.Q. Yao, Yu. Ivanisenko, T. Diemant, A. Caron, A. Chuvilin, J.Z. Jiang, R.Z. Valiev, M. Qi, H.J. Fecht, Acta Biomaterialia 6 (2010) 2816.
[8] P.J. Chu, S.Y. Wu, K.C. Chen, J.L. He, A. Yerokhin, A. Matthews, Thin Solid Films 519 (2010) 1723.
[9] D. Krupa, J. Baszkiewicz, J. Zdunek, J. Smolik, Z. Słomka, J.W. Sobczak, Surface & Coatings Technology 205 (2010) 1743.
[10] M.R. Bayati, F. Golestani-Fard, A.Z. Moshfegh, Applied Surface Science 256 (2010) 4253.
[11] J. He, Q.Z. Cai, Y.G. Ji, H.H. Luo, D.J. Li, B. Yu, Journal of Alloys and Compounds 482 (2009) 476.
[12] A. Fujishima, X. Zhang, D.A. Tryk, Surface Science Reports 63 (2008) 515.
[13] S.C. Lo, C.F. Lin, C.H. Wu, P.H. Hsieh, Journal of Hazardous Materials B114 (2004) 183.
[14] Y. Bessekhouad, D. Robert, J.V. Weber, Journal of Photochemistry and Photobiology A: Chemistry 163 (2004) 569.
[15] K. Vinodgopal, P.V. Kamat, Environmental Science & Technology 29 (1995) 841.
[16] J. Georgieva, S. Armyanov, E. Valova, I. Poulios, S. Sotiropoulos, Electrochemistry Communications 9 (2007) 365.
[17] M.D. Hernandez-Alonso, I. Tejedor-Tejedor, J.M. Coronado, J. Soria, M.A. Anderson, Thin Solid Films 502 (2006) 125.
[18] S. Stoyanov, D. Mladenova, C. Dushkin, Reaction Kinetics and Catalysis Letters 88 (2006) 277.
[19] V. Puddu, R. Mokaya, G.L. Puma, Chemical Communications 45 (2007) 4749.
[20] A.K.L. Sajjad, S. Shamaila, B.Z. Tian, F. Chen, J.L. Zhang, Applied Catalysis B: Environmental 91 (2009) 397.
[21] C.L. Yu, J.C. Yu, W.Q. Zhou, K. Yang, Catalysis Letters 140 (2010) 172.
[22] J. He, Q. Luo, Q.Z. Cai, X.W. Li, D.Q. Zhang, Materials Chemistry and Physics 129 (2011) 242.
[23] M. Miyauchi, A. Nakajima, T. Watanabe, K. Hashimoto, Chemistry of Materials 14 (2002) 4714.
[24] U.B. Mioč, M.R. Todorović, M. Davidović, Ph. Colomban, I. Holclajtner-Antunovic, Solid State Ionics 176 (2005) 3005.
[25] I.V. Lukiyanchuk, V.S. Rudnev, Inorganic Materials 43 (2007) 264.
[26] I.V. Lukiyanchuk, V.S. Rudnev, V.G. Kuryavyi, P.S. Gordienko, Russian Journal of Applied Chemistry 77 (2004) 1460.
[27] M. Petković, S. Stojadinović, R. Vasilić, I. Belča, Z. Nedić, B. Kasalica, U.B. Mioč, Applied Surface Science 257 (2011) 9555.
[28] P. Lianos, Journal of Hazardous Materials 185 (2011) 575.
[29] J. Georgieva, E. Valova, S. Armyanov, N. Philippidis, I. Poulios, S. Sotiropoulos, Journal of Hazardous Materials 211–212 (2012) 30.
[30] M. Hepel, I. Kumarihamy, C.J. Zhong, Electrochemistry Communications 8 (2006) 1439.
[31] I. Paramasivam, S. Singh, M. Moll, C. Hauser, K. Meyer, P. Schmuki, Electrochimica Acta 66 (2012) 7.
[32] C.R. Chenthamarakshan, N.R. de Tacconi, R. Shiratsuchi, K. Rajeshwar, Journal of Electroanalytical Chemistry 553 (2003) 77.
[33] S. Stojadinovic, I. Belca, M. Tadic, B. Kasalica, Z. Nedic, Lj. Zekovic, Journal of Electroanalytical Chemistry 619–620 (2008) 125.
[34] J.M. Albella, I. Montero, J.M. Martinez-Duart, Electrochimica Acta 32 (1987) 255.
[35] S. Ikonopisov, Electrochimica Acta 22 (1977) 1077.
[36] G. Sundararajan, L. Rama Krishna, Surface & Coatings Technology 167 (2003) 269.
[37] F.P. Treadwell, W.D. Treadwell, Kurzes Lehrbuch der analytischen Chemie in zwei Bänden. II. Band: Quantitative Analyse, 14. Aufl., Franz Deuticke, Wien, 1949.
[38] S. Moon, Y. Jeong, Corrosion Science 51 (2009) 1506.
[39] L. Ottaviano, F. Bussolotti, L. Lozzi, M. Passacantando, S.La. Rosa, S. Santucci, Thin Solid Films 436 (2003) 9.
[40] G.E. McGuire, G.K. Schweitzer, T.A. Carlson, Inorganic Chemistry 12 (1973) 2450.
[41] D. Bullet, Journal of Physics C: Solid State Physics 16 (1983) 2197.
[42] M.R. Bayati, F. Golestani-Fard, A.Z. Moshfegh, Applied Catalysis A: General 382 (2010) 322.
[43] J. Liqiang, Q. Yichun, W. Baiqi, L. Shudan, J. Baojiang, Y. Libin, F. Wei, F. Honggang, S. Jiazhong, Solar Energy Materials and Solar Cells 90 (2006) 1773.
[44] F. Kiriakidou, D.I. Kondarides, X.E. Verykios, Catalysis Today 54 (1999) 119.